Arrangements of magnetic moments in nanocrystalline $Fe_{48}Al_{52}$

K. Szymański, D. Satuła, and L. Dobrzyński*
University of Białystok, Institute of Experimental Physics, Lipowa 41 15-424 Białystok, Poland

E. Voronina and E. P. Yelsukov
Physical-Technical Institute of Ural Division of Russian Academy of Sciences (Izhevsk)

T. Miyanaga
Department of Materials Science and Technology, Faculty of Science and Technology, Hirosaki University, Hirosaki, Aomori 036-8561, Japan

(Received 2 March 2005; revised manuscript received 20 June 2005; published 6 September 2005)

Combined techniques, EXAFS, magnetization, and Mössbauer polarimetry are used to investigate the orientation of Fe magnetic moments in a $Fe_{48}Al_{52}$ disordered alloy prepared by mechanical grinding. Local Fe magnetic moments and their contributions to the net magnetization at selected external fields and temperatures were estimated. It was found that components of the Fe magnetic moments parallel to the net magnetizations reduce their values much faster with an increasing number of neighboring Al atoms than the total iron moments. Data analysis indicates that magnetic moments of Fe atoms surrounded by (7Al+1Fe) in the first coordination shell and by (1Al+5Fe) in the second coordination shell possess nonzero magnetic moments that form a noncolinear structure.

DOI: 10.1103/PhysRevB.72.104409 PACS number(s): 76.80.+y

I. INTRODUCTION

The magnetism of the Fe-Al system has attracted and still attracts the attention of many scientists. The reason is simple: the scientific literature is full of controversy concerning magnetic ordering, individual magnetic moments, and spin dynamics, particularly in alloys with Al concentrations close to 50%. To recall, with aluminum concentrations exceeding 20 at. % the average magnetic moment decreases rapidly and—from extrapolation to zero—one can expect that the ferromagnetism should disappear at about 34 at. % of aluminum. However, around and above this concentration a truly interesting situation takes place.

A. Colinear versus noncolinear order and spin frustration

In Al-rich B2-type ordered alloys typically antiferromagnetic (AF) order is claimed. This order has been suggested for alloys with Al concentrations from above 35% to 43% and for equiatomic composition in papers.[1–5] At the same time it has been noticed that, close to FeAl composition, ferromagnetic order can exist,[3] and supposedly antiferromagnetic or paramagnetic configurations can change into a ferromagnetic one upon simple filing.[1,6–9] Ferromagnetism has been also detected in disordered alloys with an Al concentrations range 40–70 at. %.[6,10–13]

For Fe concentrations close to 50 at. % a noncolinear ordering was considered by Bogner *et al.*[14] It was found there that an Fe antisite atom surrounded by 8 Fe neighbors forms a cluster with mean moment of 0.4 μ_B. Band structure calculations show, however, that for ideally ordered FeAl an average magnetic Fe moment is much larger and amounts to 0.71 μ_B. The energy of the ferromagnetic ground state was found to be 0.7 mRy (per formula unit) lower than the energy of the nonmagnetic state. The observed difference of magnetic moments was ascribed to possible noncolinear ordering. The authors of Ref. 14 found that the energy connected with a spin helix along the [100] direction is lower by 0.1 mRy/atom than the energy of a ferromagnetic state, if the spin direction is rotated from plane to plane by about 36 deg. Quite recent neutron diffraction data,[15] taken on a bcc-ordered FeAl alloy, showed the presence of incommensurate spin density waves. The length of the wave vector of SDWs in FeAl is rather short $k=2\pi/(na)$ (n ranges from 11 to 6 and $a=0.290$ nm), which means nearly parallel orientation of the nearest neighbor Fe magnetic moments.

For systems with atomic and spin disorders—in particular for nonordered metal systems with RKKY interaction—Mattis[16] considered a model in which spin-spin interactions were random in sign but did not result in frustrations. The spin system was considered as composed of two subsystems with randomly distributed antiparallel spins. The authors of Refs. 17 and 18 suggest that, in concentrated Fe-Al alloys, some iron atoms surrounded by a large number of aluminum atoms can flip their spins. It has also been shown[18] that in a nonordered system containing magnetic moments m_+ and m_- parallel and antiparallel to the net magnetization, respectively, the magnetizations are characterized by different temperature dynamics: the average m_- vanishes at $T<T_C$ due to Stoner-type excitations. The magnetization behavior of the Fe-Al system and the ideas of Refs. 16–18 indicate that concentrated Fe-Al alloys could serve as candidates for alloys exhibiting the so-called Mattis phase; however, no experimental support to this expectation has been found so far.

Studies of Fe-Al alloys by Monte Carlo techniques[19] in the Al concentrations range $0.25<x<0.50$ have showed that it is possible to account qualitatively for the transformation of a magnetic state from a ferromagnetic one to a certain spin glass state at about 34% Al. In these concentrated Fe-Al

alloys, RKKY interactions do not play an important role, unlike in the traditional diluted spin glass or cluster spin glass. The peculiar feature of this spin glass consists in the fact that frustrations arise from the positional disorder of Fe and Al atoms. The frustration is caused by n.n.n. Fe-Fe antiferromagnetic interactions. The authors[19] conclude that Fe atoms with 6 and more n.n. Al atoms are found to be frustrated in an ordered ferromagnetic state.

B. Other findings and the motivation of the present work

The controversial findings and apparent impact of various defects and inhomogeneities on the magnetic structure of bulk and nanocrystalline alloys require a more detailed investigation that will elucidate the nature of magnetism in this system. In this paper we report studies of a nanocrystalline Fe-Al alloy in the concentration close to the onset of ferromagnetism. EXAFS measurements were used to characterize its chemical short-range order. Local magnetic properties were investigated by the Mössbauer technique with circularly polarized monochromatic radiation. Our observations strongly suggest that a noncolinear magnetic order must exist in the sample studied.

II. SAMPLE PREPARATION

An Fe-Al ingot was synthesized from high-purity components (99.99% Fe and 99.99% Al) in an induction furnace in an Ar atmosphere, then homogenized in a vacuum furnace at 1400 K for 6 h. Chemical analysis showed that the Al concentration was 52.0 ± 0.5 at. %. The carbon content in the alloys was not higher than 0.03 wt. %. The ingots were milled and a fraction with a particle size of less than 300 μm was used for further mechanical treatment in a planetary ball mill "Pulverisette" (Fritsch) with vials and balls made of tungsten carbide (WC). Mechanical grinding was performed in an inert gas atmosphere in an 80 cm^3 volume vial filled with 4 g of powder and 25 balls with 10 mm diameter each. The supporting disk velocity was 450 rpm, with the vial velocity in relation to the supporting disk being 955 rpm. The milling of 10 h was enough to provide a disordered state in the Fe-Al alloys.[13] According to the measurements on a laser analyzer "Analizette-22," the particle size after milling ranged from 1 to 25 μm with an average of 6 μm.

III. X-RAY DIFFRACTION

X-ray diffraction studies were performed at room temperature using monochromatic Cu Kα radiation. The lattice parameter was 0.2916(4) nm. The x-ray diffraction pattern consists of the broadened peaks (110), (200), (211), and (220) of the bcc structure. The shape of the diffraction lines was analyzed and mean grain size of 4.0(3) nm and microstrains $\langle e^2\rangle^{1/2}=0.5(1)\%$ were found by use of the harmonic analysis.[20] Additionally, the peaks of WC, that get into the milled powders due to the wear of the vials and balls, were revealed. A phase analysis of the x-ray diffraction data showed that the WC admixture in the milled powders was 2 wt. %. The position of the most intensive diffraction lines resulting from WC agrees with the position of those for the milled WC powders under the same conditions of milling. We thus conclude that mechanical alloying of Fe-Al powder with WC does not occur.

IV. EXAFS MEASUREMENTS

The Fe K-edge EXAFS measurements were made at SPring-8 on the bending magnet beamline BL01B1 with a Si(111) fixed-exit double-crystal monochromator. The storage ring was operated at 8.0 GeV, and the ring current was 70–99 mA. Due to the double rhodium-coated mirror reflection, the higher harmonics were reduced to less than 10^{-5}. The spectra were taken at temperatures 10, 80, and 300 K in the transmission mode. Measurements were performed with two ionization chambers, filled with N_2 and mixture Ar $+N_2$ gases, registering incident intensity I_0, and transmitted intensity I, respectively. The size of the output slit was 0.8 mm by 5 mm.

To perform the correct determination of the local atomic structure parameters from EXAFS spectra, a procedure for correcting the nonuniformity of sample thicknesses using measurements of the absorption at a different temperature was developed and tested on intermetallic compounds.[21] The Debye temperature of the material was taken from Ref. 22. After correcting the experimental intensity ratio $I(E)/I_0(E)$ for sample thickness inhomogeneity, the absorption coefficient $\mu(E)$ was obtained. The procedure for calculating the normalized oscillatory part $\chi(k)$ consisted of standard steps—the subtraction of the pre-edge absorption function approximated by the Victoreen function, while a smooth atomiclike background was approximated by a cubic spline function followed by normalization. To make the conversion of $\chi(E)$ from energy to momentum spaces, an ordered FeAl intermetallic compound was used as reference material. Then, the E_0 value was estimated by matching the experimental EXAFS spectrum of FeAl and theoretical EXAFS spectrum calculated by the FEFF7 code.[23] The backscattering phase and amplitude, the central atom phase shift, the mean-free path, and the reduction factor were calculated using this code for known intermetallic compounds FeAl and Fe_3Al.

The analysis of normalized oscillatory parts $\chi(k)$, shown in Fig. 1(a), was performed in a single-scattering approximation within Tikhonov's regularization method.[24] The parameters of pair correlation functions (PCF): partial coordination numbers, $N_{\text{Fe-Fe}}$, $N_{\text{Fe-Al}}$, and the interatomic distances $R_{\text{Fe-Fe}}$, $R_{\text{Fe-Al}}$, were determined according to the scheme described in Refs. 25 and 26.

An analysis of the PCF parameters indicates the presence of a positional disorder induced by high-energy ball milling. This is in agreement with the EXAFS study of Ref. 27 on an implanted $Fe_{60}Al_{40}$ alloy. The disorder (atomic rearrangement) induced by irradiation or heavy plastic deformation was discussed in detail in Refs. 28 and 29. Our results show lower than expected (for a disordered alloy, deduced from stoichiometry) number of Fe atoms in the first coordination shell of Fe, and of Al atoms in the second shell of Fe, indicating a smaller disorder than reported in Refs. 28 and 29. This situation can be due to the fact that the concentration of the studied alloy is close to the stoichiometric composition.

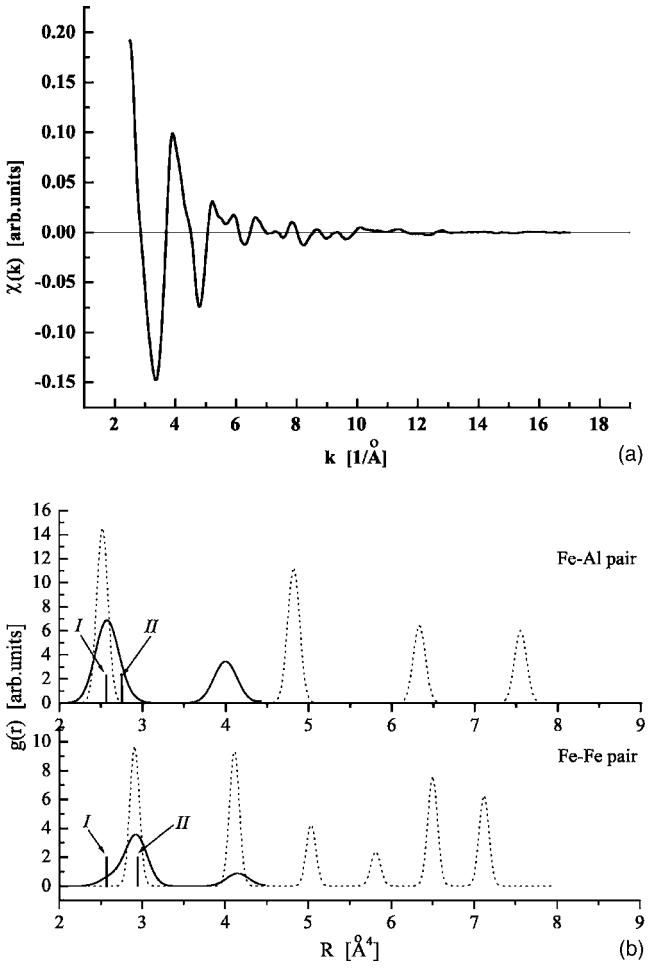

FIG. 1. (a) The EXAFS oscillatory part $\chi(k)$ taken at 10 K; (b) pair correlation functions for the disordered alloy (solid lines) in comparison with those of intermetallic compound FeAl (dashed lines). The interatomic distances for the pair correlation functions for the *I* and the *II* coordination shell are indicated by vertical bars.

The average values of interatomic distances $R_{\text{Fe-Fe}}$ for the nearest neighbors and $R_{\text{Fe-Al}}$ for the next nearest neighbors differ from the values deduced from the lattice parameter [see the vertical bars in Fig. 1(b)]. In a fully ordered alloy there are no Fe atoms in the first coordination shell of Fe and no Al atoms in the second coordination shell of Fe. In the investigated alloy with a distorted structure we observed a small number of Fe atoms in the first shell of Fe; their $R_{\text{Fe-Fe}}$ distance is 2.60 Å, larger than 2.526 Å deduced from the lattice parameter. For the Al atoms in the second shell of Fe we have found $R_{\text{Fe-Al}}=2.80$ Å, which is smaller than 2.916 Å. All these differences reflect the presence of local microdisplacements, and agree with the results of Ref. 22. The average EXAFS interatomic distance calculated from local parameters agrees to within 0.02 Å with our x ray diffraction data. Another peculiarity of the results obtained is the observed overlap of peaks in the PCF of the first and second coordination shells, which originates, first of all, from a static disorder. This cannot be caused by the poor quality of the algorithm used. Indeed, it is known that Tikhonov's regularization method, as compared to the standard Fourier transformation procedure, is of higher resolution.[25] Nevertheless, the peaks referring to the first and second distances for Fe-Fe and Fe-Al pairs in Fig. 1(b) are not resolved as well as in Fourier transformed data for FeAlMn alloys.[30]

The obtained values of $N_{\text{Fe-Fe}}$ and $N_{\text{Fe-Al}}$ correspond in terms of Cowley short-range order parameters[31] to the negative value for the first coordination shell and positive value for the second shell. The main conclusion from the EXAFS experiment is the detection of a pronounced short-range order with its quantitative characteristic $N_{\text{Fe-Fe}}$ and $N_{\text{Fe-Al}}$, presented in Table I, rather than the random distribution of atoms.

V. MAGNETIC MEASUREMENTS

Magnetic measurements were performed using a SQUID magnetometer MPMS-XL-5 (Quantum Design) in external magnetic fields up to 5 T at temperatures from 5 to 300 K. The magnetization curves and hysteresis loops were measured; FC and ZFC experiments were carried out. Magnetic measurements showed the presence of symmetric hysteresis, a lack of saturation at $T=5$ K and in fields up to 5 T (according to Ref. 6 even up to 15 T); see Figs 2 and 3. The closure of descending and ascending branches of the hysteresis loop, taking place at high B_{ext} values, $B_{ext}>0.8$ T, also gives a rather high value of coercive force $B_c\approx 50$ mT at 5 K, which falls to ≈ 3 mT at 77 K.

The average magnetic moments per Fe atom, measured at external fields B_{ext}—the same as used in a Mössbauer experiment—are shown in Table II. The data were corrected for the fraction of WC present in the sample. The magnetic ordering temperature of the sample was (110±10) K.

From an extrapolation of the high-field part of the magnetization curves to $B_{ext}=0$ we derived the value of specific magnetizations, from which the average magnetic moments per Fe atom were determined. In Fig. 4 they are presented together with the available magnetic data from literature,[9,13] and compared with the average (hyperfine magnetic field) h.m.f. obtained from Mössbauer experiments.[6,11,13] The ratio of the h.m.f. measured at a low temperature to the magnetic moments of iron inferred from magnetization measurements, is anomalously high $-29.4\ \text{T}/\mu_B$, while it is about $12.0-13.5\ \text{T}/\mu_B$ in ferromagnetic alloys with Al concentra-

TABLE I. Partial coordination numbers for the first and second coordination shells, the interatomic distances, and mean square displacements determined from of EXAFS measurements.

Shell	$R_{\text{Fe-Fe}}$ (Å)	$N_{\text{Fe-Fe}}$	$\sigma_2\times 10^2$ (Å^2)	$R_{\text{Fe-Al}}$ (Å)	$N_{\text{Fe-Al}}$	$\sigma_2\times 10^2$ (Å^2)
I	2.60±0.03	0.8±0.5	1.70	2.56±0.02	7.2±0.5	1.86
II	2.92±0.01	5.3±0.5	1.73	2.80±0.05	0.7±0.5	1.91

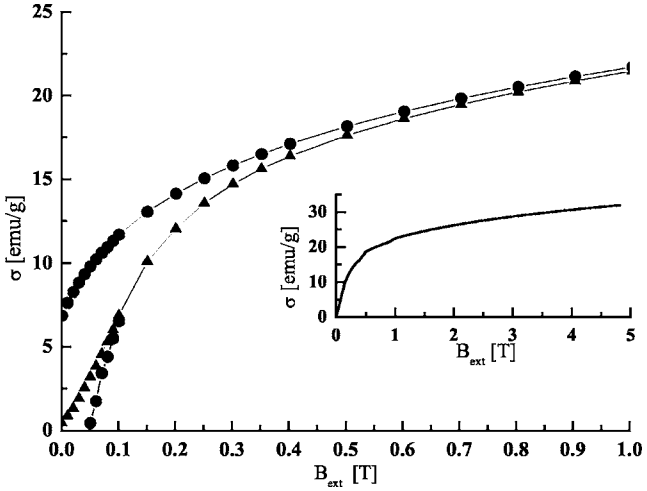

FIG. 2. The magnetization curve (triangles) and part of the hysteresis loop (circles) of the disordered $Fe_{48}Al_{52}$ measured at $T=5$ K. Inset—the magnetization curve measured in an external field up to 5 T.

tions less than 40 at. %. The temperature behavior of the magnetization measured at relatively low magnetic fields exhibits a pronounced maximum at about 40 K, Fig. 3.

VI. MÖSSBAUER SPECTROSCOPY

A. Principles of Mössbauer polarimetry

Since Mössbauer polarimetric techniques are not common, we briefly describe what physical information can be obtained from this type of measurement. ^{57}Fe h.m.f. is a vector quantity, related usually to the Fe magnetic moment. In disordered magnetic systems one encounters a distribution of both the length and the orientation of a h.m.f. vector $\mathbf{B}_{hf}$.

Preferred h.m.f. orientation, $P(\Omega)$, is usually described in a certain set of base functions, e.g., spherical harmonics Y_{lm}.[32,33] Since only M1 dipolar transitions are measured in

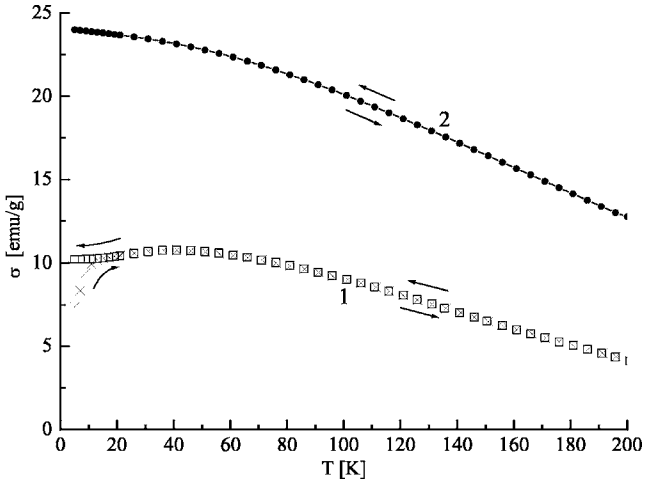

FIG. 3. ZFC (□) and FC (×) temperature dependences of the magnetization of the $Fe_{48}Al_{52}$ alloy at $B_{ext}=0.1$ T (curves 1) and $B_{ext}=1.6$ T (curves 2).

TABLE II. Magnetization, σ, and magnetic moment per Fe atom, μ_{Fe}, the average hyperfine magnetic field, $\bar{B}_{hf}$, its z component, $\bar{B}_z$, corrected for the external magnetic field, at selected temperatures and external magnetic fields.

B_{ext} (T)	T (K)	σ (emu/g)	μ_{Fe} (μ_{B})	$\bar{B}_{hf}$ (T)	$\bar{B}_z - B_{ext}$ (T)
0	13	0	0	7.9±0.1	0
0	50	0	0	4.2±0.2	0
0.2	13	12.0±2.0	0.19±0.03	7.9±0.1	−1.4±0.1
0.2	50	13.0±2.0	0.20±0.03	3.3±0.2	−0.7±0.2
1.1	13	21.4±2.0	0.33±0.03	8.2±0.1	−2.9±0.2
1.1	50	21.0±2.0	0.30±0.03	4.6±0.2	−2.2±0.2

^{57}Fe Mössbauer spectroscopy, unpolarized radiation delivers information on Y_{2m} only, while other Y_{1m} harmonics can be known when circularly polarized radiation is used. Knowledge of Y_{1m} and Y_{2m} in the texture function is equivalent to the knowledge of angular averages $\langle \boldsymbol{\gamma}_r \cdot \mathbf{m} \rangle$ and $\langle (\boldsymbol{\gamma}_r \cdot \mathbf{m})(\boldsymbol{\gamma}_s \cdot \mathbf{m}) \rangle$,[34] where $\mathbf{m}$ is an unit vector parallel to the local hyperfine field $\mathbf{B}_{hf}$, $\boldsymbol{\gamma}_r$, $\boldsymbol{\gamma}_s$ are Cartesian vectors ($r,s=x,y,z$), and brackets $\langle\ \rangle$ denote angular averaging, for any function $g(\Omega)$,

$$\langle g(\Omega) \rangle = \int_{4\pi} g(\Omega) P(\Omega) d\Omega. \tag{1}$$

In the case of a sample with axial symmetry it is convenient to choose one of the $\boldsymbol{\gamma}_r$, denoted by $\boldsymbol{\gamma}$, parallel to the $\mathbf{k}$ vector of the photon. Then the averages $\langle \boldsymbol{\gamma} \cdot \mathbf{m} \rangle \equiv c_1$ and $\langle (\boldsymbol{\gamma} \cdot \mathbf{m})^2 \rangle \equiv c_2$ can be measured with monochromatic, circularly polarized radiation.[34,35] Parameter c_2 is the average cosine square of the angle between the h.m.f. and the given direction $\boldsymbol{\gamma}$. Mössbauer absorbers prepared from powder sample exposed to an external axial magnetic field exhibit axial sym-

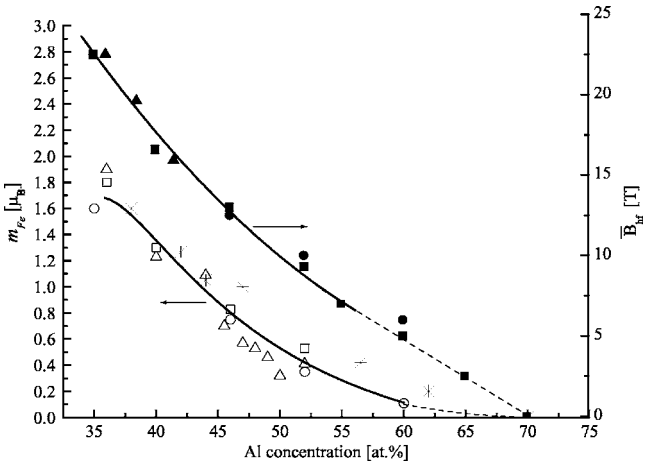

FIG. 4. The average magnetic moment per Fe atom obtained from extrapolation of high-field magnetization measurements and average hyperfine field from Mössbauer experiments ▲ (Ref. 9), △ (Ref. 6); □, ■ (Ref. 13), (×) (Ref. 11); ○, ● the authors data published in Ref. 76.

metry. Thus, in the case of a texture with axial symmetry, c_2 is a measure of the perpendicular component of the h.m.f.: $c_2=0$ means that the perpendicular component has achieved its maximum, while this component is zero when $c_2=1$. It follows from Eq. (1) that $c_1 B_{hf}$ is the average component of the h.m.f. in the $\boldsymbol{\gamma}$ direction. If we assume that, to within reasonable accuracy the atomic magnetic moment is proportional to the h.m.f., the c_1 parameter gives element-selective information about the contribution of the element to total magnetization.[36] Recently this type of information was exploited in synchrotron experiments with nuclear scattering of circularly polarized radiation.[37]

For the case of single $\mathbf{B}_{hf}$ and measurements with circularly polarized radiation, the line intensity i_n of the nth nuclear transition in the Zeeman sextet was given in Ref. 38. One can show that, having a distribution of directions of vector $\mathbf{B}_{hf}$, the expressions for i_n should contain already introduced averages, namely,

$$16i_1 = 48i_4 = 3(1 \pm 2c_1 + c_2),$$

$$4i_2 = 4i_5 = 1 - c_2,$$

$$48i_3 = 16i_6 = 3(1 \mp 2c_1 + c_2). \tag{2a}$$

We recall that, for unpolarized radiation, the line intensities are

$$16i_1 = 48i_3 = 48i_4 = 16i_6 = 3(1 - c_2),$$

$$4i_2 = 4i_5 = 1 - c_2. \tag{2b}$$

Finally, the absorber can be measured in a way that the obtained spectrum will be equivalent to a measurement on a sample with no magnetic texture[39,40] and the line intensities for such a texture-free mode are:

$$4i_1 = 6i_2 = 12i_3 = 12i_4 = 4i_6 = 1. \tag{2c}$$

B. Measurements

Texture-free absorbers for Mössbauer spectroscopy were prepared by mixing $Fe_{48}Al_{52}$ powder with Li_2CO_3 and epoxy. The measurements were performed on samples cooled in a closed cycle refrigerator equipped with an antivibration shroud. We have used absorbers containing 9.40±0.23 and 13.16±0.35 mg of $Fe_{48}Al_{52}/cm^2$. Since no available data on the temperature dependence of a recoilless fraction for disordered Fe-Al were known to us, we approximated $f_{\text{Fe-Al}}(T)$ by

$$f_{\text{Fe-Al}}(T) = f_{\alpha\text{-Fe}}(T)\frac{f_D(T,\theta_{\text{Fe-Al}})}{f_D(T,\theta_{\alpha\text{-Fe}})}, \tag{3}$$

where $f_D(T,\theta)$ is a recoilless fraction in harmonic approximation with Debye temperature θ, and $f_{\alpha\text{-Fe}}$ is a recoilless fraction of α-Fe determined in the precise experiment of Ref. 41. Debye temperatures for disordered $Fe_{48}Al_{52}$ and α-Fe were taken from Ref. 22. Finally, we estimated that the Mössbauer thickness τ (Ref. 42) of the measured absorbers were 2.60±0.07 and 3.65±0.10 at 298 K. Similarly, at $T=13$ K the thicknesses τ were 3.16±0.08 and 4.43±0.11, respectively.

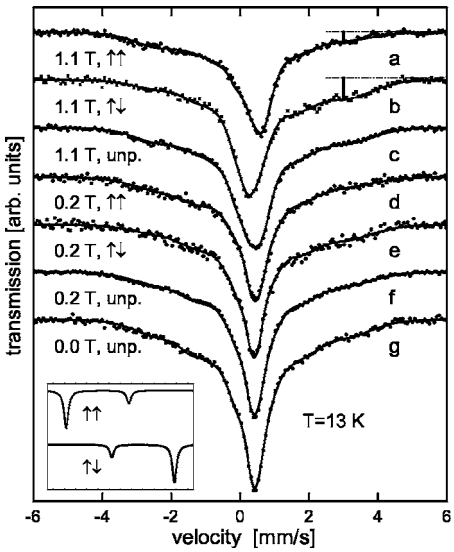

FIG. 5. Mössbauer spectra measured at $T=13$ K with polarized and unpolarized radiation in the axial applied magnetic field. Induction of the field is given on the left. Arrows ↑↑ and ↑↓ indicate two opposite circular polarizations. Solid lines represent a simultaneous fit with the same set of QS, IS, and intensities. Inset: schematic shape of the spectra of α-Fe absorber in an external magnetic field.

The absorbers were placed inside one of the rare earth magnets, producing an axially symmetric field perpendicular to the absorber surface and parallel to gamma rays. The measurements were performed at temperatures $T=13$, 50, and 298 K and external fields between 0 and 1.3 T; see Figs. 5–7.

The velocity scale of the spectra was calibrated with respect to α-Fe at room temperature. The source of unpolarized radiation was ^{57}Co in a Cr matrix. Circularly polarized monochromatic radiation was produced by the resonant filter technique.[35,43–45] The polarization degree was estimated as in Ref. 35. Additionally, we have prepared a set of α-Fe absorbers with different thicknesses and different magnetic textures. The magnetization curves for all absorbers were mea-

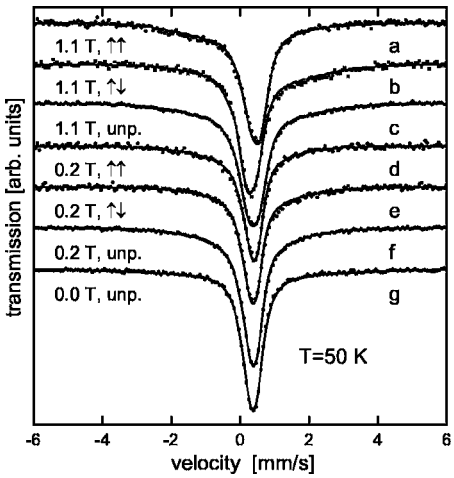

FIG. 6. The same as in Fig. 5 for $T=50$ K.

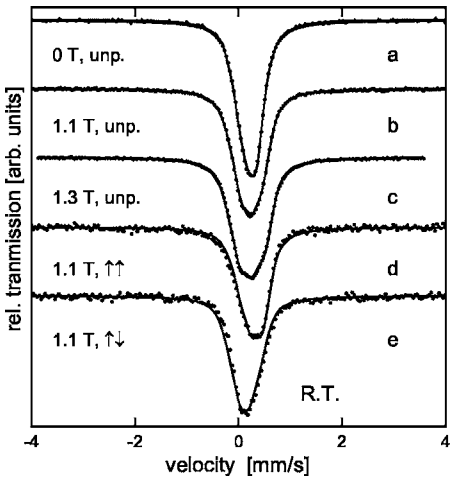

FIG. 7. Room temperature Mössbauer spectra measured with unpolarized (a)–(c) and polarized radiation (d), (e) in an external axial field. Induction of the field is given on the left. Arrows ↑↑ and ↑↓ indicate two opposite circular polarizations. Solid lines are results of a simultaneous fit with the same set of QS, IS and intensities for spectra shown in (a), (b), (c).

sured in external fields up to 3 T to obtain a fully saturated state. At a given B_{ext} the magnetization ratio $\sigma(B_{ext})/\sigma(\infty)$ is equal to the c_1 parameter. These measurements allow us to check whether nuclear polarimetry and magnetic measurements produce consistent results.

Usually the three measurements were performed at a given temperature and on an external magnetic field: with unpolarized radiation and with two opposite circular polarizations. An additional experiment in a zero applied field supplied magnetic texture-free results.

A quick inspection of these results shows that when a circular polarization state of radiation is changed to an opposite one, a clear shift of the position of the central absorption line is observed [see Figs. 5(a), 5(b), 6(a), 6(b), 7(d), and 7(e)]. It is also evident that the absorption in the region of +3 mm/s in Fig. 5(b) is larger than that one in Fig. 5(a) [see the vertical bar in Fig. 5(b), which is almost two times longer than the bar in Fig. 5(a)] while in the region of −3 mm/s the absorption in Fig. 5(a) is larger than in Fig. 5(b). From this behavior, one immediately concludes that large Fe magnetic moments (and related large hyperfine fields) are oriented as in Fe-based ferromagnets (see the inset in Fig. 5), i.e., parallel to the net magnetization. Because of the presence of a distribution of h.m.f. it is not obvious how the small hyperfine fields are spatially arranged.

C. Description of the data handling

A normalized Mössbauer spectrum $S(v)$ consists of a linear combination of N subspectra $s(v,B_i)$:

$$S(v) = \sum_{j=1}^{N} p_j s(v,B_j), \tag{4}$$

where v is Doppler velocity, and p_j is the non-negative coefficient for a field B_j. Subspectrum $s(v,B)$ is a Zeeman sextet,

$$S(v,B) = \sum_{n=1}^{6} i_n L_n(v,B), \tag{5}$$

where $L_n(v,B)$ describes the shape of the absorption line corresponding to the nth nuclear transition. Every subspectrum $s(v,B_j)$ is characterized by its relative area proportional to p_j and the two already introduced averages c_{1j} and c_{2j}. In the algorithm used by us it is possible to decompose a set of spectra, measured with different polarization states of photons, into components that fulfill Eqs. (2). Physically possible sets of p_j, c_{1j}, and c_{2j} have to be considered only, namely,

$$0 \leqslant p_j, \quad -1 \leqslant c_{1j} \leqslant 1, \quad 0 \leqslant c_{2j} \leqslant 1, \quad c_{1j}^2 \leqslant c_{2j}. \tag{6}$$

The last inequality in (6) is the Buniakovsky-Schwartz relation applied to the distribution of cosine and cosine square; see Ref. 46 for details. Equations (2) show that four types of measurements—with an unpolarized beam, with two opposite circular polarizations, and in a texture-free mode—can be simultaneously fitted with a set of p_j, c_{1j}, and c_{2j}, ($j=1,N$), fulfilling the conditions of inequalities (6).[47]

Instead of using a discrete sum of Zeeman components, we have found that a better description can be obtained by using a sum of components with a Gaussian distribution of h.m.f. This set of functions is widely used in commercially available Mössbauer packages. In our case, the use of Gaussian components permits one to obtain a continuous distribution of the h.m.f. $p(B)$, and two functions: $c_1(B)$ and $c_2(B)$.

The treatment described so far can be applied to cases where pure magnetic interactions are present. The treatment of mixed dipole magnetic and quadrupole electric interactions coupled to circularly polarized radiation have been described in Ref. 34 Using intensity tensor formalism[48–53] we have adopted expressions, Eqs. (2), to the case of mixed interactions under the assumption that the axes of the electric field gradient tensor are oriented randomly in space. In the special case of unpolarized radiation, Eqs. (2b) and (2c) and a single h.m.f. value, our algorithm is equivalent to the full Hamiltonian treatment described in Ref. 54.

Mössbauer transmission spectra are described quantitatively by the transmission integral.[42] Thickness effects were included by the folding method:[55] the cross section for resonant scattering multiplied by the effective thickness τ enters as an argument of an exponential function and was convoluted with the Lorentzian function. In all presented fits (Figs. 5–7) thickness effects are included.

D. Results of the analysis

In the first step of analysis of the Mössbauer data we determined hyperfine interactions of the alloy at room temperature. As already discussed, it was assumed that the principal axes of the electric field gradients acting on ^{57}Fe nuclei are randomly oriented. Because the sample is in a paramagnetic state, the single value of the h.m.f. equal to the external magnetic field is acting on the system, like in Ref. 54. Successful simultaneous fits to the spectra measured in different external magnetic fields [Figs. 7(a) and 7(c)] were obtained assuming the presence of four components with isomer

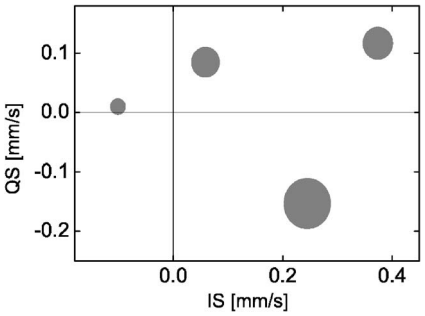

FIG. 8. Isomer shift and quadrupole splitting of four components obtained from simultaneous fits to room temperature data. The surface of the symbol is proportional to the intensity of the respective component.

shifts, quadrupole splittings, and the probabilities shown in Fig. 8. Quadrupole splitting, QS, is proportional to the main component of the electric field gradient V_{zz},

$$\mathrm{QS} = \frac{e^2 Q V_{zz} c}{2E_\gamma} \sqrt{1 + \frac{\eta^2}{3}}, \tag{7}$$

where the right-hand side parameters have the usual textbook definition.[56] The asymmetry parameter η was assumed to be zero because the fitting procedure was insensitive to the value of η. We do not interpret components in Fig. 8 as resulting from well-defined chemical environments—such a two-dimensional distribution of quadrupole splitting and isomer shift represents the measured spectra relatively well.

To analyze low-temperature data, we assumed the same isomer shift and the electric field gradient, as well as their probabilities determined at room temperature. We allowed this only for the second-order Doppler shift[57] and for the appearance of the h.m.f. distribution.

In the first stage of the analysis it was assumed that hyperfine magnetic fields correspond to the colinear magnetic structure. Thus the c_1 (as well as c_2) parameter has the same value for all magnetic components. Under this assumption we were able to perform simultaneous fits (not shown) to the data measured at $T=13$ K with unpolarized radiation, while it was not possible to find a reasonable fit to data measured with polarized radiation; the best fit achieved is displayed in Fig. 9. Next, we allowed the c_1 and c_2 parameters to vary and the best results of simultaneous fits are presented in Fig. 5.

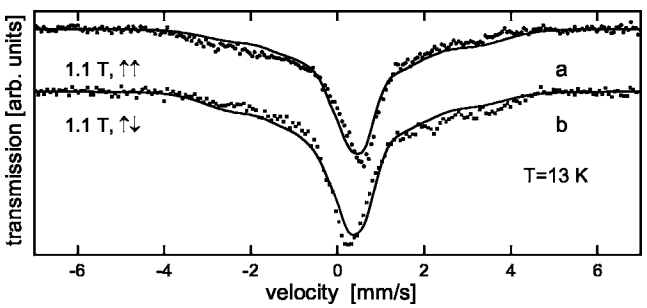

FIG. 9. Spectra measured with circularly polarized radiation and an example of the best fit under the condition that spatial orientation of the h.m.f vector does not depend on the value of h.m.f.

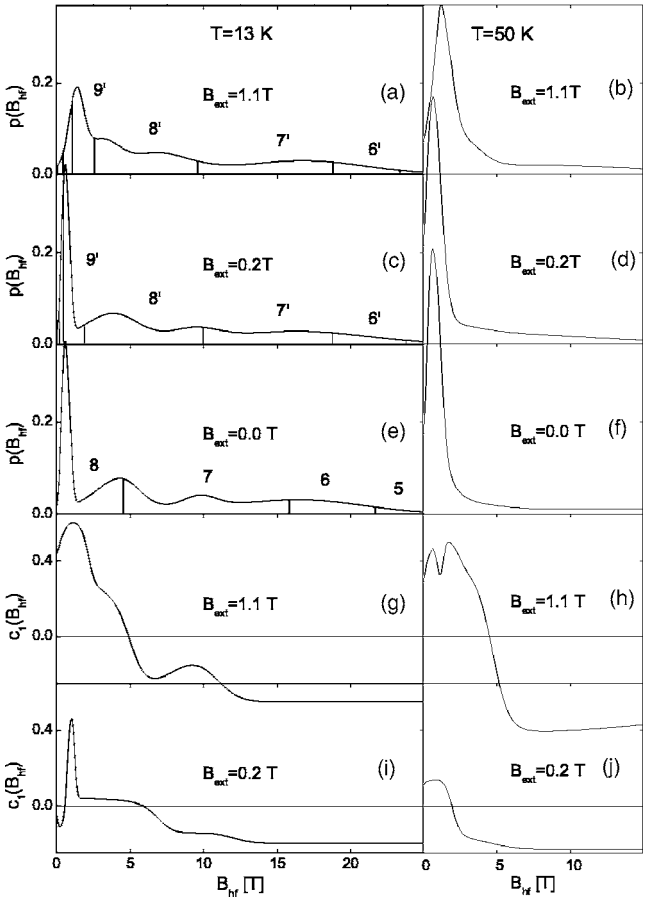

FIG. 10. Distributions of the hyperfine field measured at different values of an external an magnetic field (a)–(f) and the hyperfine field dependence of the average cosine between the hyperfine field vector and magnetization (g)–(j). Vertical bars divide $p(B_{hf})$ distribution into the sectors numbered by integers $k=8,7,6.(\ldots,9',8',7',\ldots)$ when the first (and the second) coordination shell is taken into account.

The distributions of the hyperfine fields $p(B_{hf})$ and the dependence of $c_1(B_{hf})$ are presented in Fig. 10. These dependences appeared to be almost insensitive to $c_2(B_{hf})$. Thus, the selection of $c_2(B_{hf})$ was not possible. The same treatment was used for $T=50$ K data and the results are shown in Figs. 6 and 10.

The results presented in Figs. 5, 6, and 10 can be summarized as follows. Distribution $p(B_{hf})$ has a large value in the vicinity of $B_{hf}=0$ and a tail ending at B_{hf} 30 T at $T=13$ K, and at about $B_{hf}=20$ T at $T=50$ K, which agrees with Refs. 13 and 10.

The most important result concerns $c_1(B_{hf})$ dependence. It is a known fact that the h.m.f. in the α-Fe is antiparallel to the direction of the magnetic moment of the iron atom:[58] the magnetization, i.e., the c_1 parameter, is negative. For our sample this behavior is observed only for hyperfine fields larger than about 5 T.

At $T=13$ K and a low external field, c_1 for B_{hf} smaller than approximately 5 T is small and positive. Its value decreases in the region of $B_{hf}=5-15$ T and for $B_{hf}>15$ T its value saturates. Our results indicate clearly that the average

c_1 parameter in the saturation region is larger for $T=50$ K than for $T=13$ K; compare Figs. 10(g) and 10(h).

Were the h.m.f. a monotonic function of the magnetic moment, the observed results could then be summarized as follows. The sharp peak in the $p(B_{hf})$ distribution observed close to $p(B_{hf})=0$ in the small external field and in the zero external field [Figs. 10(e) and 10(f)] corresponds to iron with a zero magnetic moment. When a larger external field is applied, we observe a shift of this peak to the B_{hf} value that is approximately equal to B_{ext}, i.e., 1.1 T [Figs. 10(a) and 10(b)], and the positive value of c_1 for the $B_{hf}=B_{ext}$ parameter [Figs. 10(g) and 10(h)] indicates that the directions of the h.m.f. and applied field coincide.

In the region close to $B_{hf}=4$ T, relatively large probability $p(B_{hf})$ is observed; see Figs. 10(a), 10(c), and 10(e). Because h.m.f. $B_{hf}=4$ T is much larger than the external field, it is reasonable to suppose that B_{hf} in this region corresponds to Fe atoms with nonzero magnetic moments. If this is so, the nearly zero value of the c_1 parameter in Fig. 10(i) indicates that these moments, on average, do not contribute to total magnetization. A similar situation is observed at $T=50$ K, $B_{ext}=1.1$ T, and B_{hf} approximately equal to 4 T [Fig. 10(b)]. One can note that the $|c_1|$ parameter for large fields [Fig. 10(h)] is larger at $T=50$ K than observed at $T=13$ K. This indicates that in the external applied field at $T=13$ K an iron subsystem with large magnetic moments is magnetically harder.

The data collected at $B_{ext}=0.2$ T should be treated more carefully. We think that the sharp peak in Fig. 10(i) and the dip in Fig. 10(h) are artefacts caused by the use of the approximated discrete hyperfine structure of QS, determined at room temperature. It is known that QS increases with decreasing temperature,[59] and the hyperfine structure in the vicinity of the zero field $p(B_{hf})$ should be interpreted with caution. However, such subtleties do not influence our main conclusions concerning the arrangements of magnetic moments.

Knowing the h.m.f. distribution, $p(B_{hf})$ and $c_1(B_{hf})$, one can calculate the average $\bar{B}_{hf}$ and average zth component $\bar{B}_z$ (to shorten notation we omit the *hf* subscript):

$$\bar{B}_{hf} = \int_0^\infty p(B)B \, \mathrm{d}B,$$

$$\bar{B}_z = \int_0^\infty p(B)c_1(B)B \, \mathrm{d}B. \tag{8}$$

Both values are given in Table II and will be discussed in the next section.

As described earlier, in the fitting procedure the isomer shift distribution at low temperatures was constrained to coincide with room temperature data. The average shift of the whole spectra was a free parameter in the fit. This is shown in Fig. 11 and compared with the second-order Doppler shift in harmonic approximation.[60] The upper curve shown in Fig. 11 corresponds to the Debye temperature already used in EXAFS data evaluation. Figure 11 indicates that consistency of data evaluation has been achieved.

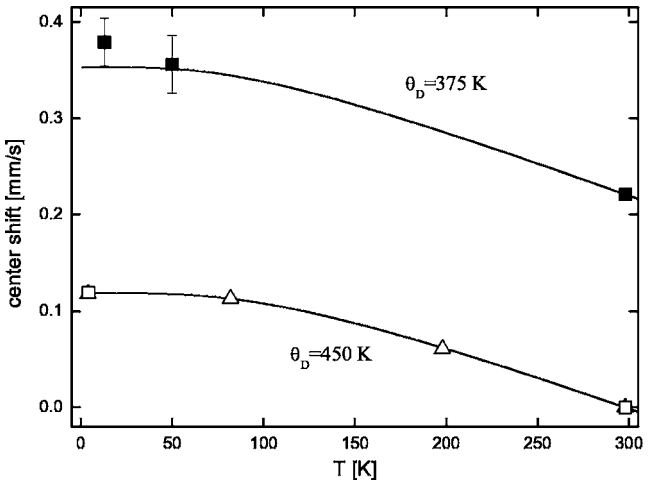

FIG. 11. Temperature dependence of the center shift. Data for α-Fe are given for a comparison. Solid lines correspond to the second-order Doppler shift in harmonic approximation with indicated Debye temperatures. △ (Ref. 77), □ (Ref. 78), ■ (this work).

VII. DISCUSSION

It is well documented that hyperfine fields and magnetic moments (or magnetization) in many ferromagnetic systems are strongly correlated. For Fe-sp-element alloys, the ratio of these two quantities is distributed in the range 10.0–15.0 T/μ_B. The data for disordered alloys of Fe with Al, Si, and P, summarized in Ref. 61, show that this factor is 12.0–13.0 T/μ_B if concentrations of the sp element in alloys do not exceed 40 at. %. The value 12.5 T/μ_B (Ref. 62) has been found in many ferromagnetic systems while it is equal to 15.2 T/μ_B for α-Fe at $T=0$.

This correlation is supported by the proportionality of core electron polarization contribution B^{cep} (proportional to the integrated spin density of *d* electrons in MT sphere, M_d) to B_{hf}. First principles calculations[63] show that the proportionality coefficient B^{cep}/M_d is 12.3 T/μ_B and does not depend either on a particular metalloid or on its concentration. Another contribution to B_{hf} comes from valence electrons and is denoted by B^{val}. In phenomenological models[3,64] this contribution is proportional to the average magnetization. If B^{val} is not too large, the relative accuracy of localized moments calculated from the aforementioned proportionality is[65] $B^{val}/(B^{cep}+B^{val})$. As was shown in Ref. 65, the dependence of B^{val} on the distance of the Fe-sp element in disordered alloys resembles RKKY polarization damped by a factor proportional to $\exp(-r_{ij}/l_0)$, where r_{ij} is the distance between Fe and impurity atoms and l_0 denotes the mean-free path of electrons. The damping term comes from substantial localization of the valence electrons. In disordered concentrated alloys with a developed density of structural defects and microdistortions, the defects also reduce considerably the RKKY interaction. According to Ref. 65 the impurities located at n.n.'s distances creates a B^{val} value not greater than 0.7 T for the first and second coordination spheres. The small value of B^{val} allows one to use the hyperfine constant B_{hf}/μ_{Fe} for the estimation of magnetic moments from the B_{hf} data, and for the interpretation of the B_{hf} distributions in terms of localized magnetic moments.

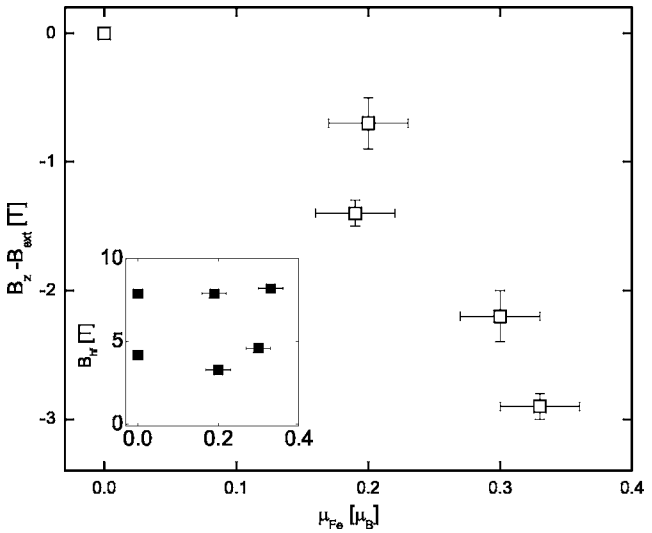

FIG. 12. The correlation between the average z component of a hyperfine field (corrected for an external field) and Fe magnetic moment (the inset shows a lack of correlation between the average h.m.f. and a magnetic moment). Open and full symbols correspond to the z component of the hyperfine field and the hyperfine field, respectively.

A considerable enhancement of the experimental value B_{hf}/μ_{Fe} (attaining values close to 30 $\mathrm{T}/\mu_{\mathrm{B}}$; see the end of Sec. V, in the Fe-Al system studied by us), can be explained as a signature of transformation from a ferromagnetic order to a nonferromagnetic one. Therefore one should expect that the magnetization should rather be correlated with the z component of the hyperfine field, B_z. This is indeed observed specifically in our alloy $\mathrm{Fe_{48}Al_{52}}$; see Fig. 12.

The resonant polarimetric technique used in the present experiment allows one to gain some insight into the local magnetic moment arrangement. The shape of the $p(B_{hf})$ distribution can be discussed in terms of a local environment model. Such a model has been successfully used in many systems, including $\mathrm{Fe_{1-x}Si_x}$, $\mathrm{Fe_{1-x}Al_x}$, in the vicinity of $x=0.25$[9,66–70] and nonordered $\mathrm{Fe_{1-x}V_x}$ alloys.[71] In these systems the Fe atoms surrounded by $(n-k)$ Fe and k non-Fe atoms in the nearest coordination shell (consisting of n atoms) contribute to well-separated peaks in the $p(B_{hf})$ distribution.[66–68,71] However, the existence of separated peaks related to well-defined local environments is not a rule, and non-Fe-rich Fe-Si and Fe-Al alloys serve as good examples of that.

It is reasonable to assume that the larger number of n.n. Fe atoms, the larger B_{hf} is observed. Next, from our EXAFS result it follows that the probabilities of finding Fe atom in the first and the second coordination shells are determined by $x_I=0.8/8$ and $x_{II}=5.3/6$, respectively. Assuming random distribution within the shells, the probability $P(k)$ that the iron atom is surrounded by $(14-k)$ Fe and k Al atoms in the two first coordination shells is

$$P(k)=\sum_{\substack{i,j\\ i+j=k;}}\binom{8}{j}\binom{6}{i}x_I^{8-j}(1-x_I)^j x_{II}^{6-i}(1-x_{II})^i \qquad (9)$$

see Table III. These assumptions allow one to divide the $p(B_{hf})$ into a few sections, each one having an area proportional to probability $P(k)$. The sectioning is displayed in Figs. 10(a) and 10(c) by vertical lines. By integration one can find the average field related to a given sector (or to the local environment),

$$\bar{B}(k)=\int_{B_k}^{B_{k+1}}p(B)B\,\mathrm{d}B\left(\int_{B_k}^{B_{k+1}}p(B)\mathrm{d}B\right)^{-1}, \qquad (10)$$

where values of B_k can be found from

$$\int_0^{B_k}p(B)\mathrm{d}B=\sum_{i=0}^{k}P(i). \qquad (11)$$

The average fields estimated according to Eq. (10) are displayed in Fig. 13 by full symbols. In a similar way we can get the average value for the z component of the hyperfine field corresponding to the kth local environment,

$$\bar{B}_z(k)=\int_{B_k}^{B_{k+1}}p(B)Bc_1(B)\mathrm{d}B\left(\int_{B_k}^{B_{k+1}}p(B)\mathrm{d}B\right)^{-1}. \qquad (12)$$

The results are shown in Fig. 13 by empty symbols. Although from Eqs. (10) and (12) one gets formally 15 numerical values of $\bar{B}_z(k)$, those for $k=0$, 1, 2, 3 and 12, 13, 14 correspond to very small probability (9) and we do not regard them as reliable. As expected, the increase of the field from $B_{ext}=0.2$ T to $B_{ext}=1.1$ T results in an increase of the B_z and not the B_{hf} values; see the empty and the strongly overlapped full points in Fig. 13.

If the influence of the second coordination shell is neglected, the binomial distribution should be used instead of (9). The results of such treatment are shown in Fig. 10(e), Table IV, and Fig. 14.

Although the results presented in Figs. 13 and 14 suffer from a different kind of approximation, they are consistent with the following picture. Let (k_1,k_2) denote an Fe atom

TABLE III. Probabilities, local magnetic moment, μ, and its z component (both within ±0.05 μ_{B}) in the external field of 0.2 and 1.1 T at $T=13$ K, for Fe surrounded by k Al and $(14-k)$ Fe atoms in the I and II coordination shells [see Eq. (9), $x_I=0.8/8=0.1$, $x_{II}=5.3/6$]. For an estimation of the total local magnetic moment, 12.5 $\mathrm{T}/\mu_{\mathrm{B}}$ was assumed.

k Al	0–4	5	6	7	8	9	10	11	12–14
$p(k)$	0.002	0.017	0.084	0.242	.368	0.213	0.062	0.010	0.001
μ (μ_{B})	—	1.98	1.65	1.15	0.43	0.10	0.04	0.01	—
μ_z (μ_{B}) ($B_{ext}=0.2$ T)	—	0.73	0.61	0.40	0.06	0.00	0.03	0.03	—
μ_z (μ_{B}) ($B_{ext}=1.1$ T)	—	1.09	0.92	0.65	0.17	0.03	0.07	0.11	—

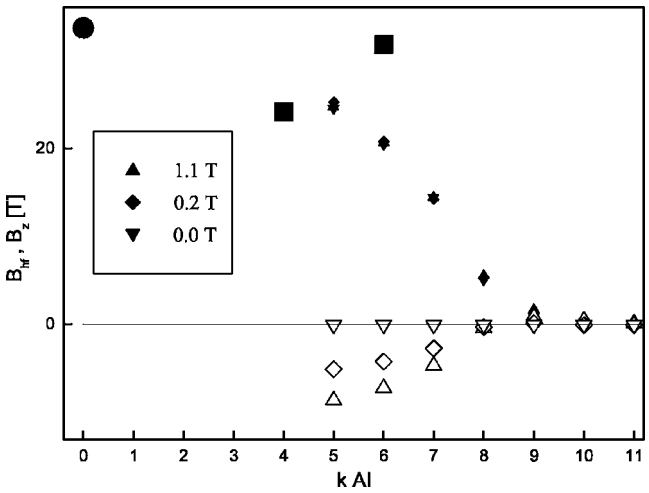

FIG. 13. Average h.m.f. and average z component of the field (not corrected for an external field) related to sectors from Fig. 10, assuming that contributions from the first and the second coordination shells to the hyperfine field are the same. Full symbols correspond to the hyperfine field; open ones to the z component of the hyperfine field. ● (Ref. 77), ■ (Ref. 64).

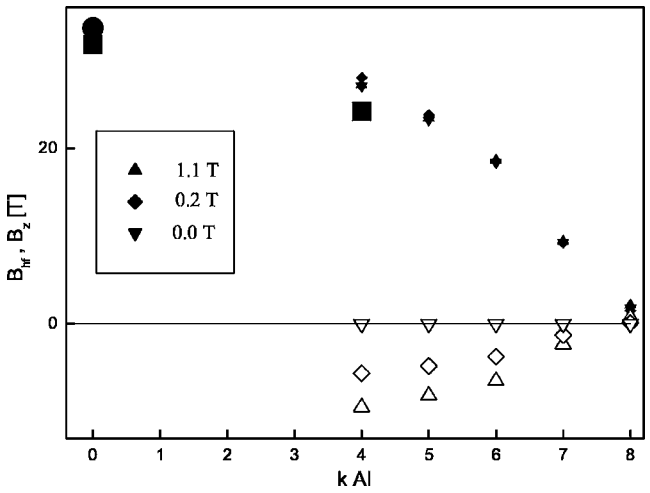

FIG. 14. The same as in Fig. 13, assuming that the contribution from the second coordination shell is neglected.

surrounded by k_1 Al atoms in the first coordination shell and k_2 Al atoms in the second coordination shell. Taking into account the most probable configurations, arbitrarily selected as those (k_1,k_2) for which the probability is greater than 5%, one observes for both models that (6,0) and (6,1) configurations have a clearly nonzero magnetic moment and a nonzero contribution to the magnetization. Configurations (8,1) and (8,2) have a clearly zero magnetic moment. Both models indicate that (7,1) has a nonzero magnetic moment and a very small contribution to the magnetization. The easiest explanation of this fact is that these configurations form a noncolinear arrangement of magnetic moments. Obviously, in Mössbauer polarimetry one measures the hyperfine field and its orientation. Thus, what can be concluded directly from our measurements is that we have evidence that the vector sum of the discussed nonzero fields is nearly zero. The noncolinear h.m.f. arrangement can be understood as a reflection of the noncolinearity of magnetic moments.

The (7,0) and (8,0) configurations could, in principle, be connected with noncolinearity. However, in light of rather poor evidence, one can also say that (7,0) configuration is connected with colinearly arranged nonzero magnetic moments, and (8,0) arrangement may have a zero magnetic moment.

Our results are consistent with a picture in which Fe atoms with a large number of Al neighbors form a noncolinear local structure at low temperatures. Noncolinearity is probably caused by local anisotropy, which may be larger than the macroscopic anisotropy observed in a single crystal.[4] Disordered moments cause large coercivity because of the interaction with a ferromagnetic matrix (neighboring magnetic moments). This is known as bias-type exchange anisotropy.[72] Under an applied external field, a gradual metamagnetic type of reorientation occurs and magnetization slowly approaches saturation. At higher temperatures thermal excitations break the magnetic ordering in Al-rich surroundings and this results in the decrease of the coercivity. Indirectly, this is confirmed by a large ($\approx$20 times) drop of coercive force as the temperature increases from 5 to 77 K, mentioned in Sec. V. One expects that the same external magnetic field will orient the ferromagnetic matrix more easily at higher (50 K) than at lower temperature (T=13 K). This is consistent with the larger value of the c_1 parameter that was obtained for T=50 K and with the maximum of magnetization observed during FC in the small magnetic field (see Fig. 3). A similar microscopic picture of the interaction was presented in Monte Carlo simulations of an Fe-Al system,[19] where Fe atoms with six and more nearest neighbor Al atoms were found to be frustrated in an ordered ferromagnetic state and where chemical disorder introduced a spin-glass-like state in the region of critical concentration.

Two different distributions of hyperfine parameters may produce identical Mössbauer spectra. This leads to the ambi-

TABLE IV. Probabilities, local magnetic moment, μ, and its z component (both within $\pm 0.05\ \mu_B$) in the external field of 0.2 and 1.1 T at T=13 K, for Fe surrounded by k Al and $(8-k)$ Fe atoms in the first coordination shell. The binomial distribution of number of Fe, Al atoms with x_I=0.8/8=0.1 was assumed. The hyperfine constant 12.5 T/μ_B was used.

k Al	0–3	4	5	6	7	8
$p(k)$	4×10^{-4}	0.005	0.033	0.149	0.383	0.430
μ (μ_B)	—	2.19	1.88	1.48	0.74	0.14
μ_z (μ_B) (B_{ext}=0.2 T)	—	0.81	0.69	0.54	0.20	0.01
μ_z (μ_B) (B_{ext}=1.1 T)	—	1.18	1.04	0.85	0.38	0.04

guity much discussed in the literature.[73–75] Additional independent experimental information usually reduces this ambiguity. It has already been demonstrated that additional information received from the polarimetric method allows one to obtain the correct shape of the h.m.f. distribution.[53] In the described algorithm one should, in principle, estimate $c_2(B_{hf})$; see Eqs. (2a) and (2b). However, in the studied case we could not obtain reasonable information about the transverse component for such strongly overlapped spectra. One can show that fits of a similar quality can be obtained for a variety of c_2 values. Because information on transverse local magnetization is not available, we do not know whether we are dealing with an antiferromagnetic order (i.e., long-range order exists to some length scale), antiparallel arrangements of moments (some iron moments at random positions are oriented antiparallel to each other), or a disordered magnetic structure if all directions of magnetic moments are present. All three possibilities are consistent with the results of our measurements.

We hope that additional measurements in the field perpendicular to the **k** vector or the use of linearly polarized radiation in which the intensity of lines 2 and 5 will be greatly enhanced, may reduce ambiguity.

The main conclusion that follows from the results presented in this report is that the arrangement of hyperfine magnetic fields is nonuniform. This kind of information could be obtained by the use of circularly polarized radiation only. The obtained result, that larger fields are better aligned in an externally applied magnetic field, is not strongly dependent on the details of data analysis. Indeed, some of the spectra were analyzed without using the transmission integral and under the assumption that the electric field gradient is zero. The main features of the $p(B_{hf})$ and $c_1(B_{hf})$ functions agree with those presented in Fig. 10.

Magnetization and Mössbauer data can be combined to obtain local magnetic moments of Fe. To estimate the z component of the magnetic moment in an external magnetic field we assume that it is proportional to $\bar{B}_z(k)$ and that the total contribution to magnetization of all Fe atoms is equal to the measured magnetization. The results are summarized in Tables III and IV.

VIII. RESUME

Combining magnetic, EXAFS, and Mössbauer polarimetric data, it was possible to get a consistent description of the arrangement of Fe magnetic moments in a $Fe_{48}Al_{52}$ alloy prepared in a structurally disordered state by mechanical grinding. The distribution of quadrupole splitting and isomer shift, determined in a RT experiment, was kept constant during low-temperature data evaluation, allowing only for the second-order Doppler shift. The Debye temperature used in EXAFS data evaluation and estimated in the diffraction experiment[22] agrees with the second-order Doppler shift found in Mössbauer data evaluation. A full Hamiltonian was used for the exact treatment of a mixed magnetic dipole and electric quadrupole interaction. The transmission integral was used for treatment of the thickness effect, and the temperature dependence of the recoilless fraction was taken into account.

We have estimated the values of Fe magnetic moments as a function of the local environment. An increase of the number of Al in the two first coordination shells (bcc structure) causes a decrease of magnetic moments and a much faster decrease of the z component of the magnetic moment (the local contribution to the magnetization). Magnetic moments of iron in configurations (6,0) and (6,1), which can be considered as iron-rich clusters, form colinear arrangement. Configuration (7,1) was found as forming a noncolinear structure. Configurations (8,1) and (8,2) are so poor in iron that either no magnetic moment is formed on the central Fe atom, or the magnetic moment is below the detection limit of our technique. One should stress that such a detailed description of the magnetic moment arrangement would hardly be possible if an extensive combination of experimental methods had not been used in the present study.

The noncolinearity present at low temperatures explains the large coercivity, lack of saturation, and anomalously large ratio of the average h.m.f. to the magnetic moment in the range of critical concentration.

ACKNOWLEDGMENTS

The authors thank Dr. A. V. Korolyov for the magnetic measurements and the staff of SPring-8 for the maintenance of the facility of JASRI Grant No. 2002A0078NX-np.

*Also at The Sołtan Institute for Nuclear Studies, 05-400 Otwock-Świerk, Poland.

[1] A. Arrott and H. Sato, Phys. Rev. **114**, 1420 (1959).
[2] H. Sato and A. Arrott, Phys. Rev. **114**, 1427 (1959).
[3] M. Shiga and Y. Nakamura, J. Phys. Soc. Jpn. **40**, 1295 (1976).
[4] H. Danan and H. Gengnagel, J. Appl. Phys. **39**, 678 (1968).
[5] G. P. Huffman, J. Appl. Phys. **42**, 1606 (1971).
[6] M. J. Besnus, A. Herr, and A. J. P. Meyer, J. Phys. F: Met. Phys. **F5**, 2138 (1975).
[7] A. Taylor and R. M. Jones, J. Phys. Chem. Solids **6**, 16 (1958).
[8] E. A. Friedman and W. J. Nicholson, J. Appl. Phys. **34**, 1048 (1963).
[9] G. P. Huffman and R. M. Fisher, J. Appl. Phys. **38**, 735 (1967).
[10] M. Shiga and Y. Nakamura, J. Physiol. Suppl. (Paris) **40**, C2 (1979).
[11] M. Shiga, T. Kikawa, K. Sumiyama, and Y. Nakamura, J. Magn. Soc. Jpn. **9**, 187 (1985).
[12] N. I. Kulikov, A. V. Postnikov, G. Borstel, and J. Braun, Phys. Rev. B **59**, 6824 (1999).
[13] E. P. Yelsukov, E. V. Voronina, and V. A. Barinov, J. Magn. Magn. Mater. **115**, 271 (1992).
[14] J. Bogner, W. Steiner, M. Reissner, P. Mohn, P. Blaha, K.

Schwarz, R. Krachler, H. Ipser, and B. Sepiol, Phys. Rev. B **58**, 14922 (1998).
[15] D. R. Noakes, A. S. Arrott, M. G. Belk, S. C. Deevi, Q. Z. Huang, J. W. Lynn, R. D. Shull, and D. Wu, Phys. Rev. Lett. **91**, 217201 (2003).
[16] D. C. Mattis, Phys. Lett. **56A**, 421 (1976).
[17] A. K. Arzhnikov and L. V. Dobysheva, J. Magn. Magn. Mater. **117**, 87 (1992).
[18] A. K. Arzhnikov and L. V. Dobysheva, Phys. Lett. A **195**, 176 (2000).
[19] G. S. Grest, Phys. Rev. B **21**, 165 (1980).
[20] B. E. Warren and B. L. Averbach, J. Appl. Phys. **21**, 595 (1950).
[21] E. Voronina, D. Guy, and T. Miyanaga, Nucl. Instrum. Methods Phys. Res. B **215**, 525 (2004).
[22] H. W. Sheng, Y. H. Zhao, Z. Q. Hu, and K. Lu, Phys. Rev. B **56**, 2302 (1997).
[23] S. I. Zabinsky, J. J. Rehr, A. Ankudinov, R. C. Albers, and M. J. Eller, Phys. Rev. B **52**, 2995 (1995).
[24] Y. A. Babanov and V. R. Shvetsov, Phys. Status Solidi B **131**, K1 (1985).
[25] Y. A. Babanov, V. V. Vasin, A. L. Ageev, and N. V. Ershov, Phys. Status Solidi B **105**, 747 (1981).
[26] E. V. Voronina, V. Fomin, Y. Babanov, and E. P. Yelsukov, Phys. Met. Metallogr. **89**, 68 (2000).
[27] T. Sikora, M. Jaouen, T. Girardeau, and J. Mimault, Nucl. Instrum. Methods Phys. Res. B **111**, 141 (1996).
[28] H. Bakker, G. F. Zhou, and H. Yang, Prog. Mater. Sci. **159**, 39 (1995).
[29] C. Suryanarayana, Prog. Mater. Sci. **46**, 1 (2001).
[30] V. G. Harris, D. J. Fatemi, K. B. Hathaway, Q. Huang, A. Mohan, and G. J. Long, J. Appl. Phys. **85**, 5181 (1999).
[31] J. M. Cowley, J. Appl. Phys. **21**, 24 (1950).
[32] H. D. Pfannes and H. Fischer, Appl. Phys. **13**, 317 (1977).
[33] H. D. Pfannes and R. M. Paniago, Hyperfine Interact. **71**, 1499 (1992).
[34] K. Szymański, Nucl. Instrum. Methods Phys. Res. B **134**, 405 (1998).
[35] K. Szymański, L. Dobrzyński, B. Prus, and M. J. Cooper, Nucl. Instrum. Methods Phys. Res. B **119**, 438 (1996).
[36] K. Szymański, D. Satuła, L. Dobrzyński, K. Perzyńska, M. Biernacka, and P. Zaleski, J. Magn. Magn. Mater. **236**, 56 (2001).
[37] C. L'abbé, J. Meersschaut, W. Sturhahn, J. S. Jiang, T. S. Toellner, E. E. Alp, and S. D. Bader, Phys. Rev. Lett. **93**, 037201 (2004).
[38] H. Frauenfelder, D. E. Nagle, R. D. Taylor, D. R. F. Cochran, and W. M. Visscher, Phys. Rev. **126**, 1065 (1962).
[39] J. M. Greneche and F. Varret, J. Phys. (France) Lett. **43**, L233 (1982).
[40] J. M. Greneche and F. Varret, J. Phys. C **15**, 5333 (1982).
[41] U. Bergmann, S. D. Shastri, D. P. Siddons, B. W. Batterman, and J. B. Hastings, Phys. Rev. B **50**, 5957 (1994).
[42] S. Margulies and J. R. Ehrman, Nucl. Instrum. Methods **12**, 131 (1961).
[43] S. Shtrikman, Solid State Commun. **5**, 701 (1967).
[44] J. P. Stampfel and P. A. Flinn, Moessbauer Eff. Methodol. **6**, 95 (1971).
[45] F. Varret, P. Imbert, G. Jehanno, and R. Saint-James, Phys. Status Solidi A **27**, K99 (1975).
[46] K. Szymański, D. Satuła, and L. Dobrzyński, J. Phys.: Condens. Matter **11**, 881 (1999).
[47] K. Szymański, D. Satuła, and L. Dobrzyński, Hyperfine Interact. **156/157**, 21 (2004).
[48] R. Zimmermann, Chem. Phys. Lett. **34**, 416 (1975).
[49] U. Gonser and H. Fischer, in *Mössbauer Spectroscopy II* (Springer-Verlag, Berlin, 1981), p. 99.
[50] R. Zimmermann, in *Advances in Mössbauer Spectroscopy Applications to Physics, Chemistry and Biology* (Elsevier, Amsterdam, 1983).
[51] H. Spiering, in *Mössbauer Spectroscopy Applied to Inorganic Chemistry* (Plenum, New York, 1984), Vol. 1, p. 77.
[52] K. Szymański, J. Phys.: Condens. Matter **12**, 7495 (2000).
[53] K. Szymański, Nucl. Instrum. Methods Phys. Res. B **171**, 515 (2000).
[54] N. Blaes, H. Fischer, and U. Gonser, Nucl. Instrum. Methods Phys. Res. B **9**, 201 (1985).
[55] T. M. Lin and R. S. Preston, Moessbauer Eff. Methodol. **9**, 25 (1974).
[56] N. N. Greenwood and T. C. Gibb, *Mössbauer Spectroscopy* (Chapman and Hall Ltd., London, 1971).
[57] B. D. Josephson, Phys. Rev. Lett. **4**, 341 (1960).
[58] S. S. Hanna, J. Heberle, G. J. Perlow, R. S. Preston, and D. H. Vincent, Phys. Rev. Lett. **4**, 513 (1960).
[59] B. Kolk, in *Studies of Dynamical properties of Solids with the Mössbauer Effect* (North-Holland, Amsterdam, 1984).
[60] K. N. Shrivastava, Phys. Rev. B **1**, 955 (1970).
[61] E. P. Yelsukov, Y. N. Vorobyov, T. I. Arbusova, and I. B. Smolyak, J. Magn. Magn. Mater. **130**, 44 (1994).
[62] P. Panissod, J. Durand, and J. I. Budnick, Nucl. Instrum. Methods Phys. Res. **199**, 99 (1982).
[63] A. K. Arzhnikov and L. V. Dobysheva, Phys. Rev. B **62**, 5324 (2000).
[64] C. E. Johnson, M. S. Ridout, and T. E. Cranshaw, Proc. Phys. Soc. Jpn. **81**, 1079 (1963).
[65] A. K. Arzhnikov, L. V. Dobysheva, and F. Brouers, Phys. Solid State **42**, 89 (2000).
[66] M. B. Stearns, Phys. Rev. **129**, 1136 (1963).
[67] M. B. Stearns, J. Appl. Phys. **35**, 1095 (1964).
[68] V. Niculescu, T. J. Burch, and J. I. Budnick, J. Magn. Magn. Mater. **39**, 223 (1983).
[69] P. A. Beck, Metall. Trans. **2**, 2915 (1971).
[70] B. Fultz, Z. Q. Gao, and H. H. Hamdeh, Hyperfine Interact. **54**, 521 (1990).
[71] J. C. Krause, J. Schaf, M. I. da Costa, Jr., and C. Paduani, Phys. Rev. B **61**, 6196 (2000).
[72] A. E. Berkowitz and K. Takano, J. Magn. Magn. Mater. **200**, 552 (1999).
[73] G. L. Caër, J. M. Dubois, H. Fischer, I. U. Gonser, and H. G. Wagner, Nucl. Instrum. Methods Phys. Res. B **5**, 25 (1984).
[74] G. L. Caër and R. A. Brand, J. Phys.: Condens. Matter **10**, 10715 (1998).
[75] D. G. Rancourt, in *Mössbauer Spectroscopy Applied to Magnetism and Materials Science* (Plenum, New York, 1996), Vol. 5, p. 105.
[76] E. P. Yelsukov, E. V. Voronina, A. V. Korolyov, and G. N. Konygin, NATO Sci. Ser. II Math. Phys. Chem. **94**, 93 (2003).
[77] C. E. Violet and D. N. Pipkorn, J. Appl. Phys. **42**, 4339 (1971).
[78] R. S. Preston, S. S. Hanna, and J. Heberle, Phys. Rev. **128**, 2207 (1962).